Cambridge Centre for Computational Chemical Engineering

University of Cambridge

Department of Chemical Engineering

Preprint ISSN 1473 – 4273

A Detailed Chemistry Multi-cycle Simulation of a Gasoline Fueled HCCI Engine Operated with NVO

Jonathan Etheridge [1] , Sebastian Mosbach [1] , Markus Kraft [1] , Hao Wu [2] , Nick Collings [2]

released: 9 January 2009

[1] Department of Chemical Engineering
University of Cambridge
New Museums Site
Pembroke Street
Cambridge, CB2 3RA
UK
E-mail: mk306@cam.ac.uk

[2] Department of Engineering
University of Cambridge
Trumpington Street
Cambridge, CB2 1PZ
UK

Preprint No. 64

c4e

Key words and phrases: HCCI engine modelling, detailed chemistry, NVO

Edited by
Cambridge Centre for Computational Chemical Engineering
Department of Chemical Engineering
University of Cambridge
Cambridge CB2 3RA
United Kingdom.

Fax: + 44 (0)1223 334796
E-Mail: c4e@cheng.cam.ac.uk
World Wide Web: http://www.cheng.cam.ac.uk/c4e/

Abstract

A previously developed Stochastic Reactor Model (SRM) is used to simulate combustion in a four cylinder in-line four-stroke naturally aspirated direct injection Spark Ignition (SI) engine modified to run in Homogeneous Charge Compression Ignition (HCCI) mode with a Negative Valve Overlap (NVO). A portion of the fuel is injected during NVO to increase the cylinder temperature and enable HCCI combustion at a compression ratio of 12:1. The model is coupled with GT-Power, a one-dimensional engine simulation tool used for the open valve portion of the engine cycle. The SRM is used to model in-cylinder mixing, heat transfer and chemistry during the NVO and main combustion. Direct injection is simulated during NVO in order to predict heat release and internal Exhaust Gas Recycle (EGR) composition and mass. The NO_x emissions and simulated pressure profiles match experimental data well, including the cyclic fluctuations. The model predicts combustion characteristics at different fuel split ratios and injection timings. The effect of fuel reforming on ignition timing is investigated along with the causes of cycle to cycle variations and unstable operation. A detailed flux analysis during NVO unearths interesting results regarding the effect of NO_x on ignition timing compared with its effect during the main combustion.

Contents

1 Introduction **3**

2 Model Details **5**

3 Model Calibration **6**

3.1 Fuel Split 6

3.2 Injection Timing 10

4 Results and Discussion **12**

4.1 Cyclic Variation and Instabilities 12

4.2 Fuel Reforming 14

4.3 NO Effect on Combustion Phasing 18

4.4 NO_x in the NVO 19

5 Conclusion **24**

1 Introduction

The widespread use of Internal Combustion Engines (ICE) and growing concerns over climate change have made it necessary to improve the efficiency and emissions of modern engines. HCCI has shown potential as an alternate ICE operating mode that offers low NO_x and particulate emissions and high efficiency. Unlike SI and Compression Ignition Direct Injection (CIDI) engines, in which combustion is initiated with a spark or fuel injection, there is no direct ignition control in HCCI. The in-cylinder temperature, pressure and composition at Inlet Valve Closing (IVC), and to a lesser extent the turbulence, determine the combustion phasing, making HCCI more difficult to control than conventional operating modes. To accurately model HCCI combustion it is therefore beneficial to use a detailed chemical mechanism. Probability Density Function (PDF) based models have proven advantageous for simulating HCCI combustion due to their ability to incorporate detailed chemistry whilst maintaining low computational times [1].

Several different strategies for achieving stable HCCI have been investigated including; heating the intake air [2], boosting the intake pressure [3], varying the compression ratio [4] and the use of dual fuels or fuel additives [5]. The application of alternative fuels, such as n-butane, propane, ethanol etc., has also been explored [3].

There are still problems with HCCI operation. Due to the low combustion temperatures, HCCI operation can produce high CO and unburned hydrocarbon (UHC) emissions. Currently HCCI can only be used within a narrow operating range. The low load limit occurs when the fuel concentration is too low to be ignited properly causing unstable operation. During startup the charge is too cold for HCCI operation. At high loads the large rates of heat release lead to engine knock.

A possible solution is to switch back to a conventional mode of operation at certain loads. The transition from SI or CIDI to HCCI is challenging due to the different temperatures and exhaust gas composition in each of the modes of operation [6, 7]. Switching from HCCI to another mode is less problematic, however it is still important to obtain a smooth transition [8].

To achieve HCCI combustion at compression ratios used in SI engines a NVO can be used to trap exhaust gas in the cylinder, and utilize its thermal energy to raise the IVC temperature [9, 10]. It also dilutes the charge, reducing the rate of heat release, making it possible for higher loads to be achieved without knock. EGR increases the heat capacity of the charge, which reduces the effect of air temperature on combustion [11] and reduces the peak combustion temperature, helping to prevent NO_x formation [12]. The use of internal EGR causes each cycle to rely on the temperature and exhaust gas composition of the previous cycle. It was found that oscillatory cycles can occur when a late combustion is quenched, causing a large amount of UHC to be present in the residual gas which burns during NVO advancing the following cycle's combustion phasing [10].

Certain exhaust species retained by EGR may have a large influence on the combustion in the following cycle. At high EGR ratios, combustion duration may be shortened by CO_2 and H_2O [13]. It has also been suggested that H_2O advances ignition timing by a chemical effect [12]. It was found that low concentrations of NO caused combustion phasing to advance [14, 15]. It was suggested that NO advances combustion by the production of the reactive OH radical as shown in reaction (1).

$$HO_2\cdot \quad + \quad NO \quad \rightleftharpoons \quad OH\cdot \quad + \quad NO_2 \tag{1}$$

The use of direct injection (DI) enables the amount and timing of fuel injection to be varied as well as allowing multiple injections per cycle. Injecting a fraction of the fuel during NVO and the remainder during intake is a promising strategy for controlling HCCI. This has been found to increase the lean limit and reduce fuel consumption [16]. It produces a nearly homogeneous mixture which results in an efficient, stable and fast combustion [17]. The early injection can also result in reduced NO_x and UHC emissions for the same reason [18]. Injecting during NVO can increase pumping losses from the drop in cylinder temperature and pressure as the fuel evaporates [19]. The opposite effect can be observed when heat is released during the NVO expansion [18]. The reactions that take place have also been reported to increase the fuel's ignitability and advance the combustion phasing [20–22]. This effect is known as fuel reforming and can expand the lean limit of combustion without increasing NO_x emissions [16]. Advancing the NVO injection timing or increasing the fraction of fuel injected can advance the main combustion phasing due to increased NVO heat release and fuel reforming [20–22]. The magnitude of control these strategies offer is however highly dependent on the amount of O_2 available during NVO [23].

Simulations can be used to gain further insight into the complex processes occurring in HCCI engines and may be used for optimizing control [24]. When a large amount of EGR is used, multi-cycle simulations are required to couple consecutive cycles. PDF based models can be used with detailed chemistry at relatively low computational cost making them a useful tool for multi-cycle engine simulation.

The paper is structured as follows. Details of the model are described in the next section. The following section shows results from the calibrated model. Simulation and experimental results are then compared at various split ratios and injection timings. Next an investigation into the causes of cycle to cycle variations (CCV) and unstable operating conditions is presented. The effect of fuel reforming is then discussed and some interesting results regarding the effect of NO_x on combustion phasing are shown. Conclusions are drawn in the final section.

2 Model Details

The previously developed Stochastic Reactor Model (SRM) [1, 25, 26] has been used to simulate an HCCI engine operated with a 146 CAD NVO. The model is based on the PDF transport equation [27] and uses the Euclidean Minimum Spanning Tree (EMST) mixing model [28]. The model also contains stochastic heat transfer and direct injection sub-models. A detailed Primary Reference Fuel (PRF) chemical mechanism containing 157 species and 1552 reactions was used.

Details of the engine are given in Table 1. A split injection strategy was used, in which 20-40 % of the fuel was injected during NVO, referred to as pilot injection. The pilot injection timing was also varied. The second injection took place during the intake stroke and was assumed to result in a homogenous mixture at IVC. For this reason all particles at IVC were given the same composition and temperature. The cooling effect of spray evaporation was accounted for at IVC. The compositions at IVO and EVO were stored and used as the EGR composition at the following closed valve event. The mass and composition of EGR at IVO was also stored and used as the mass and composition of EGR at IVC. It was assumed that any EGR lost through the intake valve is re-inducted during the next intake stroke and that the difference in its composition and mass between consecutive cycles is small enough to cause no effect. Due to fluctuations in air and EGR mass in each cycle, the fuel mass rather than equivalence ratio was set and the EGR mass instead of ratio was used. The SRM was coupled with GT-Power, a one dimensional engine simulation tool, to enable multi-cycle simulation. GT-Power was used to model heat and mass flow through the engine during the intake and exhaust events. Each case was run for 40 cycles with 100 stochastic particles.

Table 1: *Engine specifications.*

Cylinders	4
Fuel	95 RON gasoline
Bore [mm]	87.5
Stroke [mm]	83.0
Con. rod length [mm]	146.3
Disp. volume [cm^3/cyl]	499
CR	12
IVO [CAD BTDC]	295
IVC [CAD BTDC]	125
EVO [CAD ATDC]	109
EVC [CAD ATDC]	279
Start of main inj. [CAD BTDC]	260

3 Model Calibration

The different operating conditions modelled are given in Table 2. The base case, case 1, was used to calibrate the engine model parameters. Cases 2 and 3 had different fuel split ratios compared to the base case. The fuel split ratio is the mass of fuel supplied in the main injection divided by the total amount used per cycle. Cases 4 and 5 had different pilot injection timings to the base case.

Table 2: *Engine operating conditions.*

Case	1	2	3	4	5
Fuel split	0.8	0.7	0.6	0.8	0.8
Pil. inj.[CAD ATDC]	315	315	315	305	285
Fuel [mg/cyl/cyc]	9.77	9.85	9.90	9.75	9.78
λ	1.33	1.32	1.31	1.32	1.29
Speed [RPM]	1511	1511	1511	1510	1513
BMEP [bar]	2.62	2.61	2.61	2.60	2.59

Figure 1a shows the average pressure profiles during the main combustion of case 1 for 40 simulated and 200 experimental cycles. The simulation matches experimental data well. The NVO pressure profiles are compared in Figure 1b and suggest the simulated heat release during NVO is slightly lower and occurs later than it does in the experiment. Peak pressures against the crank angle they occurred for forty consecutive cycles are compared with experimental results in Figure 2. Peak pressures occur slightly earlier in the simulation than the experiment. The average fuel air equivalence ratio obtained in the simulation was 1.25, compared with a measured value of 1.33. This value is important as a poor match would suggest incorrect EGR mass and temperatures at IVC and EVC. Emissions data is given in Table 3. The NO_x result suggests temperatures in the simulation were a good match to the experiment. The model contains a crevice but no wall impingement sub-model, which could be one cause of the low UHC and CO emissions obtained in the simulation. The engine was also operated in SI mode at the same speed and load with an injection timing of 308 CAD BTDC, producing 3120 ppm UHC and 4900 ppm CO. These are very close to the HCCI values suggesting that wall impingement could be a major cause of UHC and CO in the engine. The UHC emissions should not have a direct impact on the following combustion due to the fuel injected during NVO, however the NVO heat release may be effected. Consecutive cycles did not appear to show a trend as can be seen by comparing peak pressures in Figure 3. This result agreed with the experimental data.

3.1 Fuel Split

The fuel split ratio was varied in cases 1-3 as shown in Table 2 with the other parameters the same as in Table 1. All model parameters used were kept constant apart from the

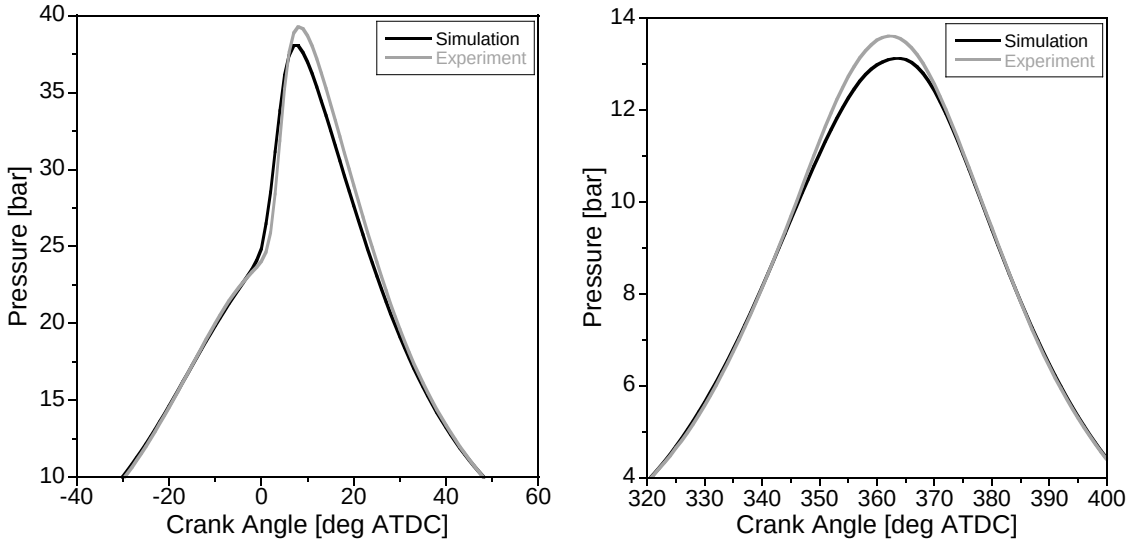

(a) (b)

Figure 1: *Average pressure profile during main combustion and NVO of 40 simulated and 200 experimental cycles of case 1.*

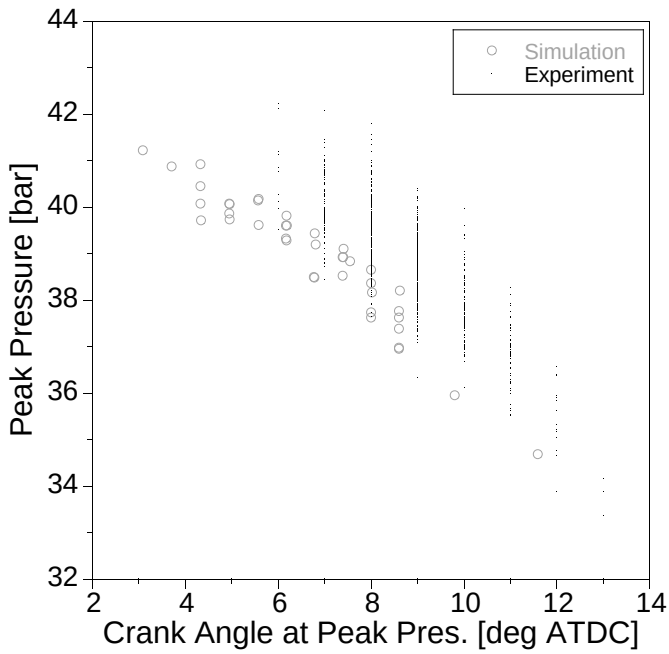

Figure 2: *Peak pressure against the crank angle it occurs for 40 simulated and 200 experimental cycles of case 1.*

Table 3: *Average emissions over 200 experimental and 40 simulated cycles (33 cycles for case 3).*

Case	1	2	3	4	5
NO_x [ppm] Exp.	15.2	20.5	24.7	14.3	16.9
NO_x [ppm] Sim.	8.0	9.9	10.9	8.0	7.8
CO [ppm] Exp.	1032	1008	1029	964	956
CO [ppm] Sim.	13.1	244.3	115.2	281.2	89.4
UHC [ppm] Exp.	2958	2789	2604	2924	2974
UHC [ppm] Sim.	8.5	57.2	30.5	65.2	22.1

values given in Table 2, which were varied in the experiments. Figure 4a shows a decrease in the fuel split ratio caused an advance in combustion phasing. The same trend was seen in the simulation as shown in Figure 4b. The average peak pressure was however lower with lower fuel split ratios, which did not occur in the experiment. This was probably due to a larger variation in combustion phasing in the simulations and the effect of averaging the pressure profiles.

Table 4: *Average results over 40 cycles (33 cycles for case 3).*

Case	1	2	3	4	5
Lambda	1.25	1.24	1.23	1.25	1.25
Lambda NVO	1.02	0.93	0.85	1.02	1.02
IVC T [K]	503.5	503.9	502.8	504.3	506.1
EVC T [K]	695.0	697.5	697.3	695.9	694.4
NVO heat rel. [J]	43.1	43.5	42.7	43.6	45.2
CA50 [deg ATDC]	3.6	3.5	3.3	4.1	2.9
Internal EGR [%]	48.2	48.1	48.0	48.2	48.1

The advance in combustion phasing has been reported in the literature as due to increased NVO heat release and due to the fuel becoming more reactive from reactions during NVO. The average IVC temperatures in cases 1-3 are given in Table 4 and show only a slight variation as does the NVO heat release. This suggests the reason for advanced combustion phasing is the fuel reforming effect. The NO_x emissions increased as more fuel was injected during NVO, matching the experimental trend. This is probably due to combustion occurring closer to TDC resulting in higher temperatures. By comparing Tables 4 and 2, it can be seen that the air fuel equivalence ratio decreased with a decrease in fuel split ratio, which was also observed in the experiment. Figure 5 shows the NVO pressure profiles in the experiment and simulation for the three cases. The pressure before TDC is lower when the fuel mass injected during NVO is increased. This was due to the evaporation of the fuel cooling the charge. The effect of varying fuel split ratio is investigated further in the Fuel Reforming section.

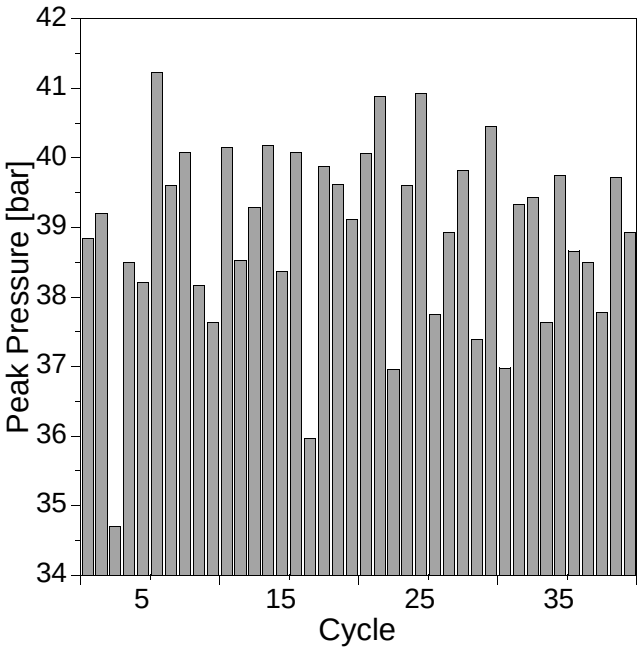

Figure 3: *Peak pressure against the cycle it occurs for 40 simulated cycles of case 1.*

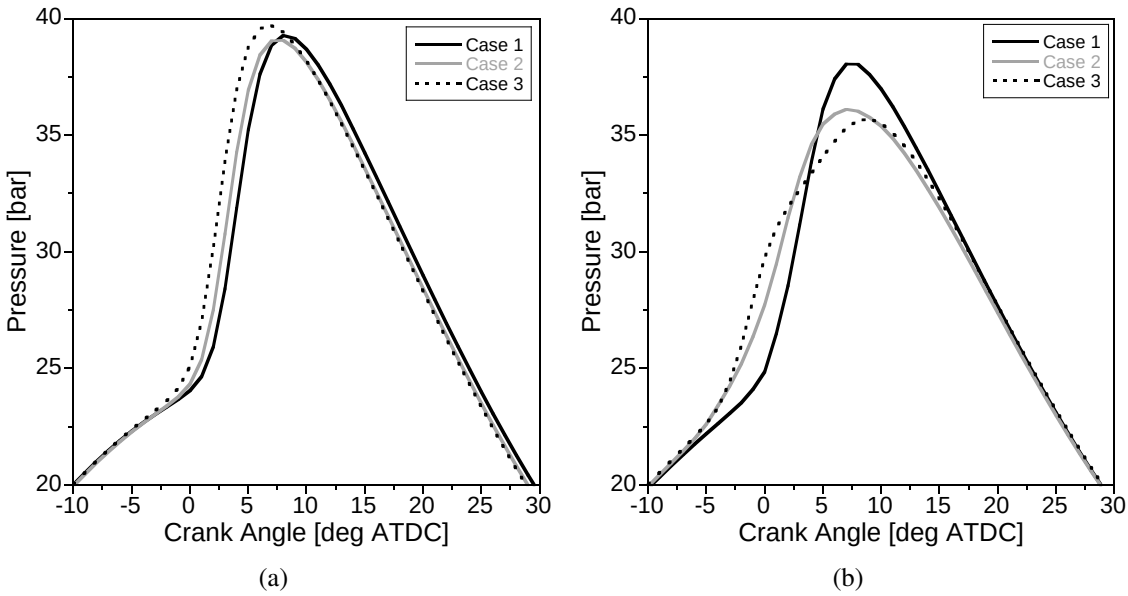

Figure 4: *Average combustion pressure profiles over (a), 200 experimental cycles for cases 1-3, and (b), 40 simulated cycles for case 1 and 2, and 33 cycles for case 3.*

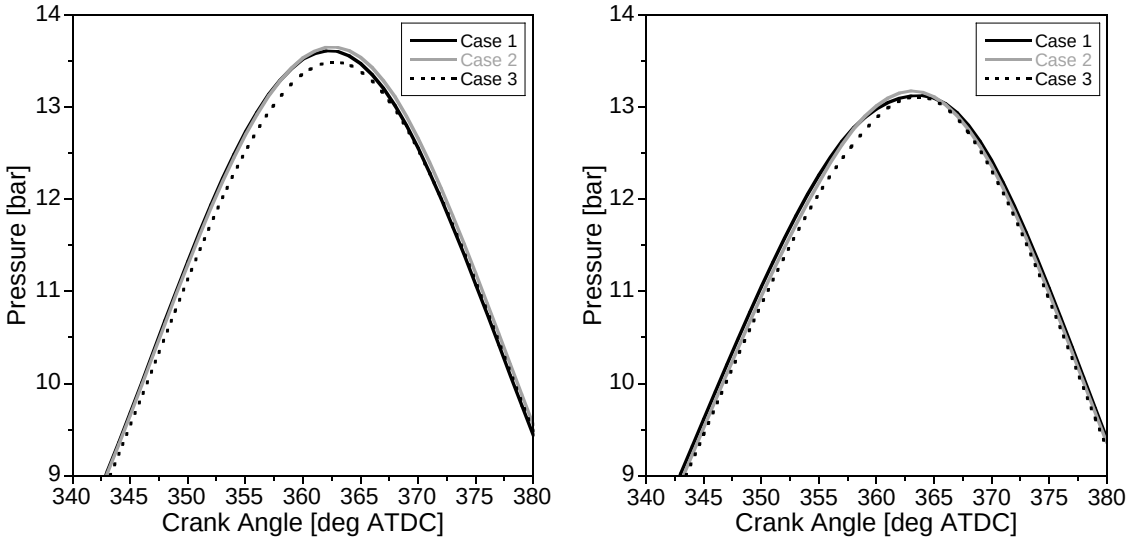

(a) (b)

Figure 5: *Average NVO pressure profiles over (a), 200 experimental cycles for cases 1-3, and (b), 40 simulated cycles for case 1 and 2, and 33 cycles for case 3.*

The average pressure profiles and values for case 3 are only for the first 33 cycles as a misfire occurred in cycle 34. This will be discussed in the Cyclic Variation and Instabilities section.

3.2 Injection Timing

The pilot injection timing was varied in cases 1, 4 and 5 as shown in Table 2 with the other parameters the same as in Table 1. All model parameters were kept constant apart from the values given in Table 2, which were varied in the experiments. Figure 6a shows an advance in pilot injection timing caused an advance in combustion phasing. The same trend was seen in the simulation as shown in Figure 6b.

The average IVC temperatures increased as the pilot injection timing was advanced. This was due to increases in NVO heat release, given in Table 4. Figure 7 shows the NVO pressure profiles in the experiment and simulation for the three cases. The peak pressure increased as the pilot injection timing was advanced due to increased heat release. The increase in NVO heat release is caused by an increase in the fuels residence time in the cylinder. This will lead to a less stratified mixture and allows more time for reactions to occur.

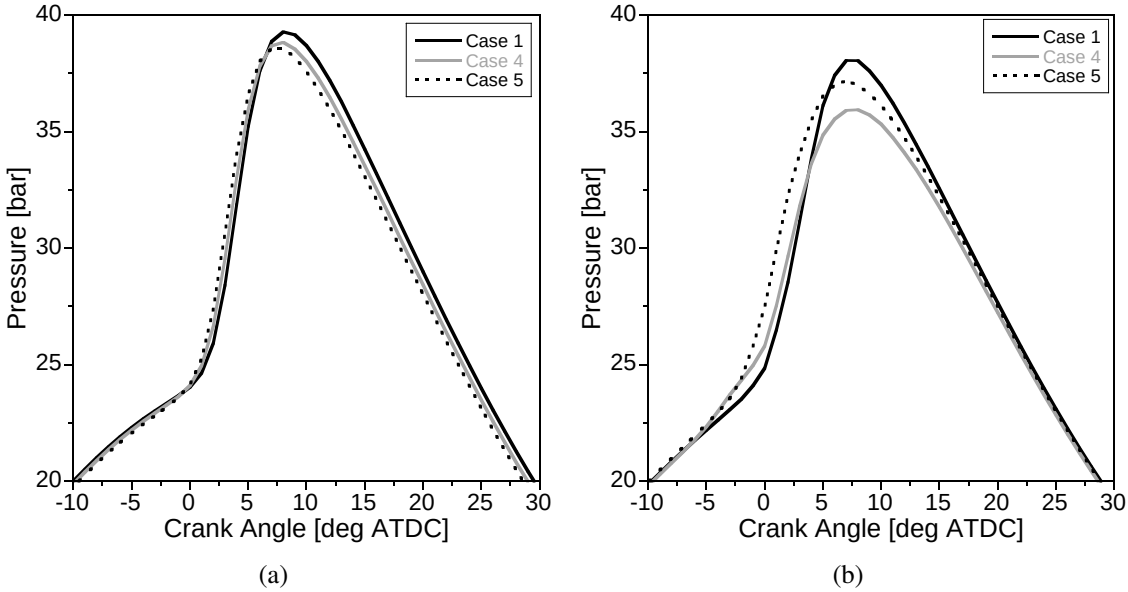

Figure 6: *Average combustion pressure profiles over (a), 200 experimental cycles and (b), 40 simulated cycles for cases 1, 4 and 5.*

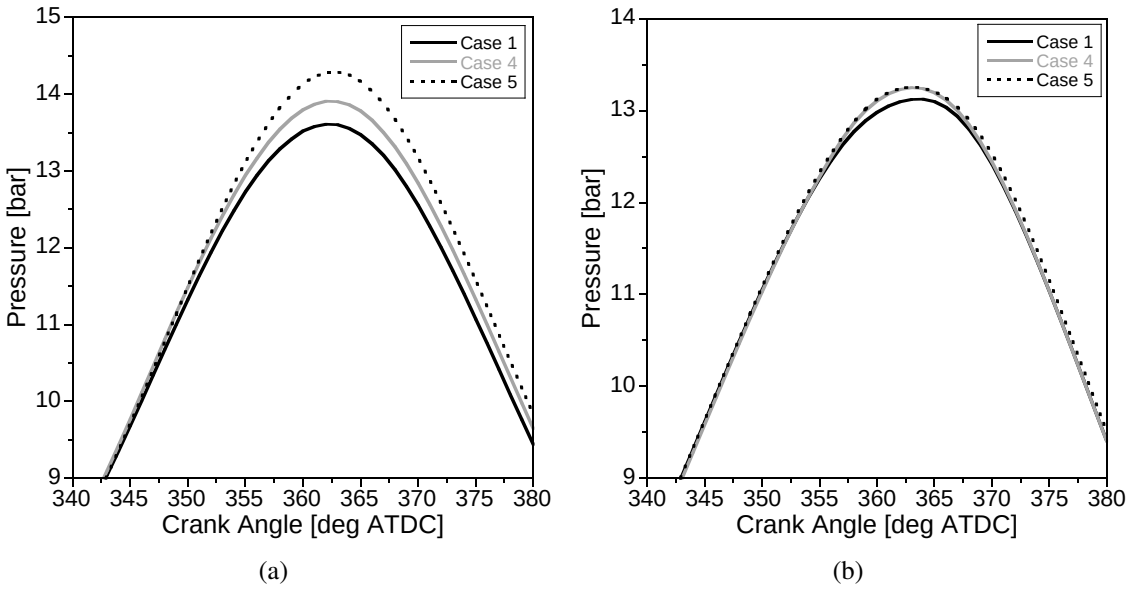

Figure 7: *Average NVO pressure profiles over (a), 200 experimental cycles and (b), 40 simulated cycles for cases 1, 4 and 5.*

4 Results and Discussion

For all of the cases the simulation showed larger CCV and slightly advanced average combustion phasing. The gasoline fuel was simulated with a PRF mechanism. Due to the high temperature and low pressure experienced at IVC and EVC in an HCCI engine with NVO, it is likely the octane index (OI) of the fuel will be lower than the actual RON. It is also likely that it will be lower during NVO compared to the main combustion due to the higher temperature at similar pressure. A PRF mixture with a RON of 60 was used for both so it may be true that a higher main combustion PRF RON should have been used which may have delayed the start of combustion bringing the simulations more in line with the experiment. Another problem was with case 3 where a large amount of fuel was injected during NVO. The actual fuel split comes from the ratio of injector voltage pulse widths during each injection. It is likely that the actual ratio of pilot fuel to total fuel was lower due to the delay before the fuel flowrate through the injector reaches its maximum taking up a higher percentage of injection time for a shorter injection period. Further investigations into the results are discussed in the following sections.

4.1 Cyclic Variation and Instabilities

The simulation of case 3 started well but then large CCVs developed which ended in complete misfire as can be seen in Figure 8. The cycles fluctuate between high and low peak pressures corresponding to early and late combustion phasing. From Figure 9 it can be seen that heat release during NVO fluctuated between values centred at 30 J and 60 J. The heat release during NVO has a strong impact on IVC temperature which in turn has a large impact on combustion phasing. The cause of misfire in the simulation of case 3 was a low IVC temperature resulting from too low heat release during NVO.

Figure 9 shows no trend between EVC temperature and NVO heat release. The equivalence ratios after pilot injection fall into clusters centred at 1.19 and 1.15 at heat release values of 30 J and 60 J respectively. This suggests the mass of O_2 trapped at EVC limits the NVO heat release observed in the simulation. Figure 10 shows the 40 consecutive fuel air equivalence ratios during NVO after the pilot injection. The values alternate between close to 1.15 and 1.19. This can explain the oscillating peak pressures observed. High IVC temperatures are caused by a large amount of NVO heat release. A high IVC temperature causes an advanced combustion phasing and a high peak pressure. The high IVC temperature also reduces the mass of air inducted during the intake stroke. This in turn causes low NVO heat release due to limited O_2 availability and a retarded combustion phasing in the following cycle. The simulated fuel air ratio was slightly richer than the measured value (see Tables 2 and 4) which could explain why the simulation became unstable and the experiment did not.

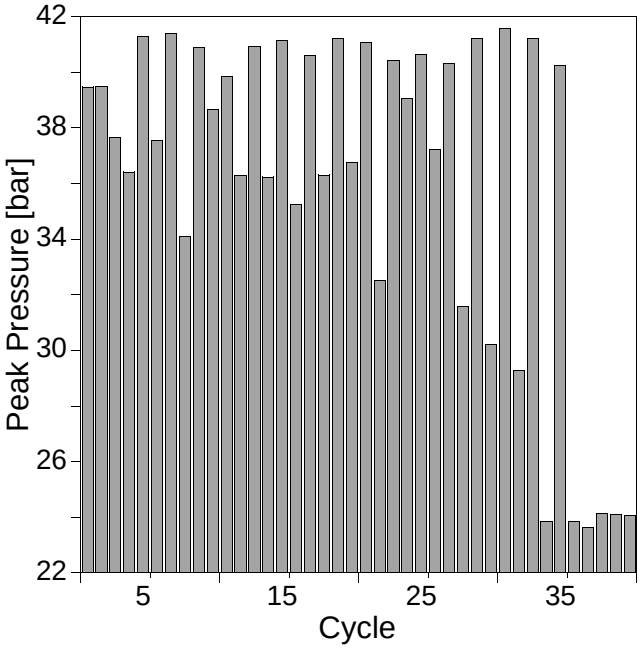

Figure 8: *Peak pressure against the cycle it occurs for 40 simulated cycles of case 3.*

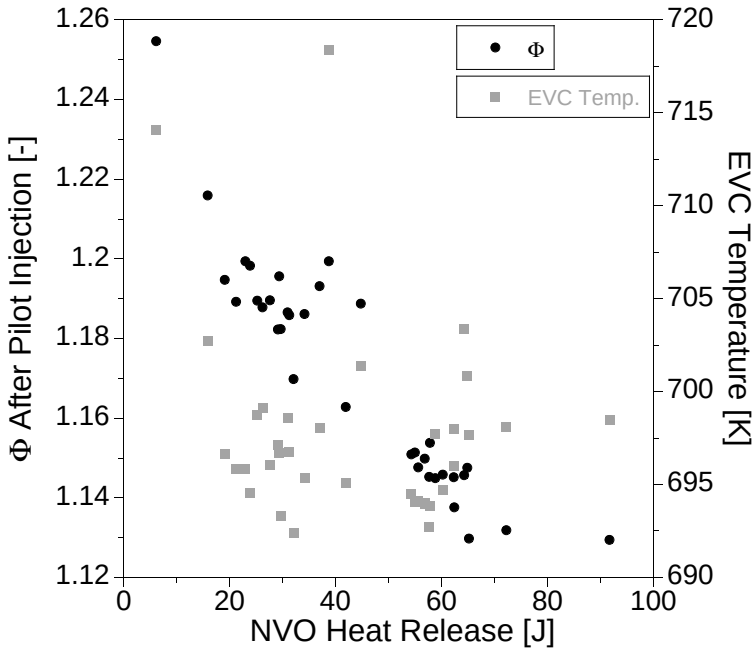

Figure 9: *The fuel air equivalence ratio after pilot injection and EVC temperature against the heat released during NVO for 40 simulated cycles of case 3.*

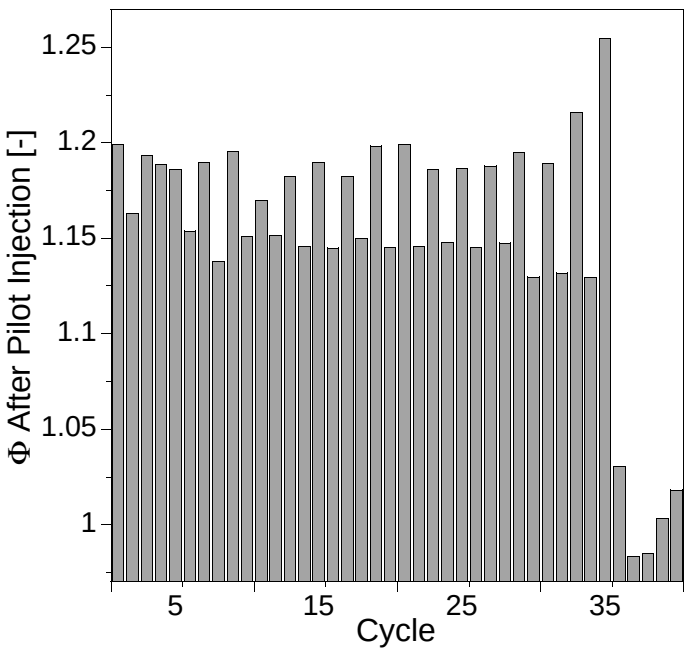

Figure 10: *Fuel air equivalence ratio after NVO injection against the cycle it occurs for 40 simulated cycles of case 3.*

4.2 Fuel Reforming

The calibrated model was used to investigate the effect of fuel reforming. NVO simulations of case 1 were run with varying air mass fractions. The temperature at EVC was 694 K and the composition was taken from a combustion cycle with a peak pressure close to the average. Figure 11 shows that an increase in the oxygen mass during NVO results in more NVO heat release which agrees with the analysis in the previous section. The mass fraction of carbon species containing different numbers of carbon atoms are compared for the 0.94 and 1.03 fuel air equivalence ratio cases in Figure 12. The compositions are given at 10 CAD after pilot injection, when the fuel had evaporated, and at IVO. The figure shows the C7 and C8 mass fractions decrease during NVO as the PRF injected is split into smaller molecules. The richer case maintains higher C7 and C8 mass fractions as the reactions do not proceed as far as in the lean case. The C5 and C6 mass fractions increase in the rich case and decrease in the lean case. Mass fractions of C2 to C5 increase in both cases but to a higher extent in the rich case. In the rich case the CO and CO_2 mass fractions increased by 5.7×10^{-3} and 4.8×10^{-4} respectively. In the lean case the CO and CO_2 mass fractions increased by 1.0×10^{-2} and 1.3×10^{-2} respectively.

The compositions at IVO were then used in identical combustion simulations to asses the chemical effect of the reformed fuel on combustion phasing. An IVC temperature of 503.5 K was used in all of the simulations. Comparing Figures 11 and 13 shows an increase in NVO heat release caused the combustion phasing to retard. The results suggest the further the reactions proceed during NVO, the less reactive the charge becomes.

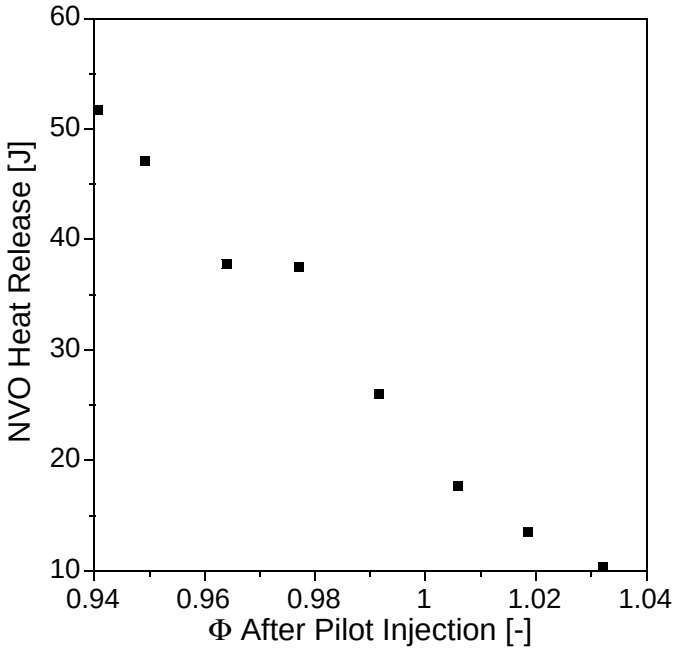

Figure 11: *Heat released during NVO at different EVC air mass fractions.*

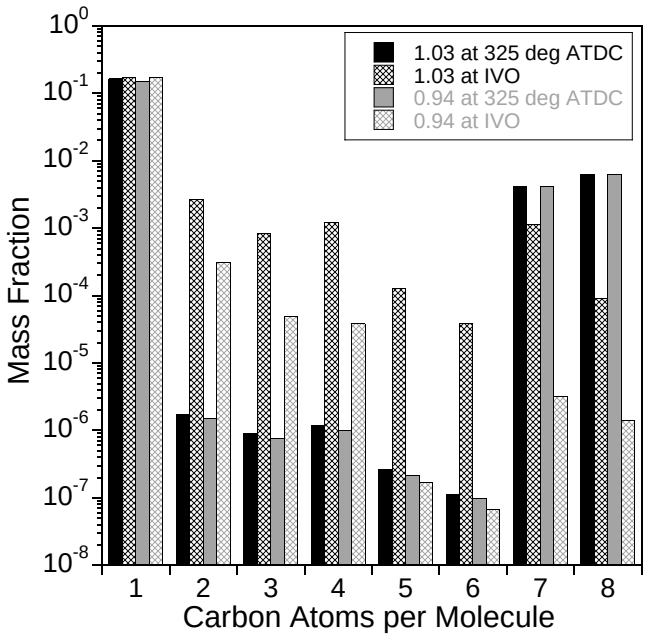

Figure 12: *Mass fractions of carbon species 10 CAD after pilot injection and at IVO at fuel air equivalence ratios 0.94 and 1.03 after pilot injection.*

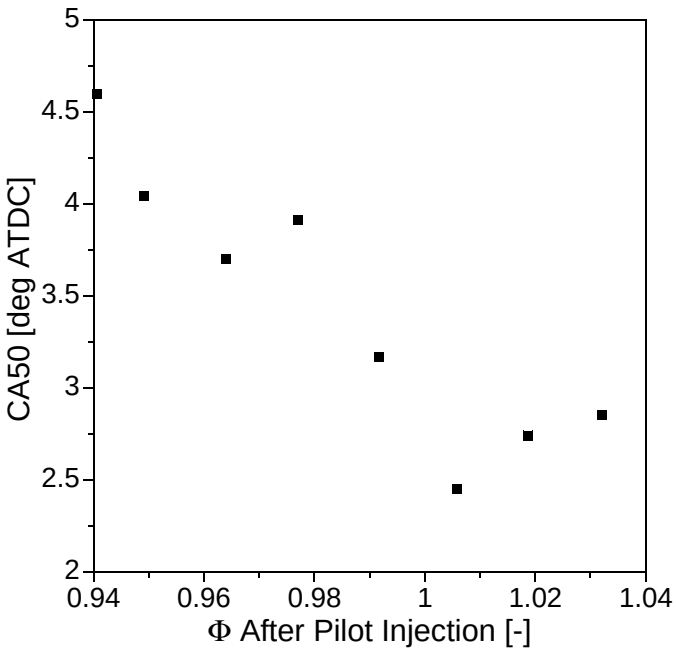

Figure 13: *CA50 during main combustion using EGR from NVOs with different EVC air mass fractions.*

The same combustion EVO composition, total fuel mass and EVC temperature used in the previous NVO parameter sweep was used in simulations with different fuel split ratios. The EVC air mass fraction was the same as for the 0.99 ϕ after pilot injection case. No trend was seen in the NVO heat release as shown in Figure 14. The simulations resulted in similar NVO heat release. To obtain the same heat release when more fuel is injected suggests the reactions did not progress as far. Figure 15 compares the mass fractions of C1-C8 species just after pilot injection and at IVO for the 0.81 and 0.59 fuel split ratio cases. The figure shows the reactions in the 0.81 fuel split case proceed further than in the 0.59 case. The CO and CO_2 mass fractions increased by 1.2×10^{-2} and 2.9×10^{-3} respectively in the 0.81 fuel split ratio case. In the 0.59 fuel split ratio case the CO and CO_2 mass fractions increased by 1.3×10^{-2} and 2.8×10^{-3} respectively.

Figure 16 compares the CA50 when the IVO compositions from the NVO simulations were used, along with the remaining fuel, in combustion simulations with IVC temperatures of 503.5 K. The figure suggests a decrease in fuel split ratio causes an advance in combustion phasing. When the fuel split ratio was 0.75 the NVO heat release was much lower than the other cases. This resulted in an advanced combustion phasing similar to the 0.59 fuel split case. The heat released during NVO per mass of pilot fuel injected was 7120 J/g and 8220 J/g in the 0.59 and 0.75 cases respectively. The results suggest that lower NVO heat release per mass of pilot fuel injected results in a more reactive charge. A combustion simulation was run with the same EGR mass but the composition was that used at EVC. All of the fuel was added to investigate the combustion phasing without fuel reforming. The CA50 for this case was 1.3 deg ATDC. This case was also run with the

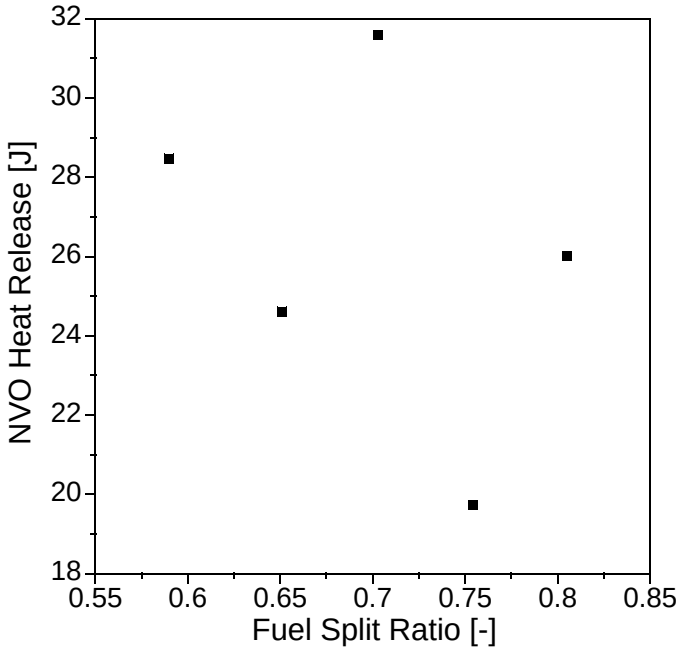

Figure 14: *Heat released during NVO with different fuel split ratios.*

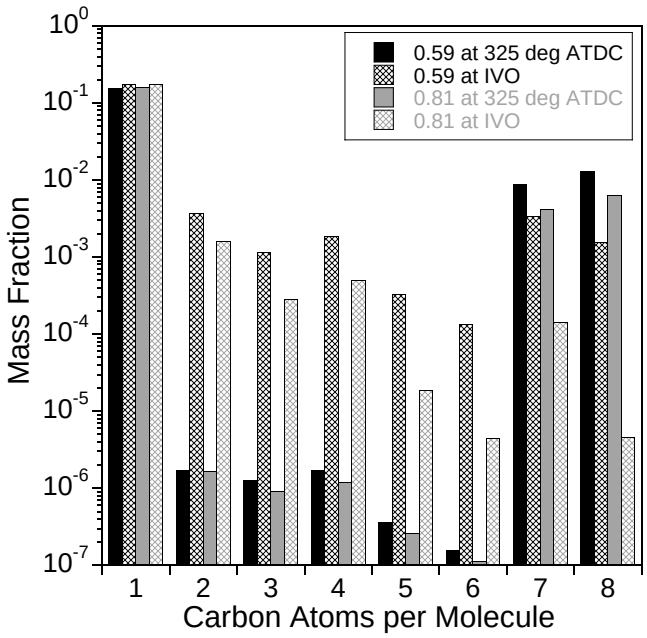

Figure 15: *Mass fractions of carbon species 10 CAD after pilot injection and at IVO at fuel split ratios 0.59 and 0.81.*

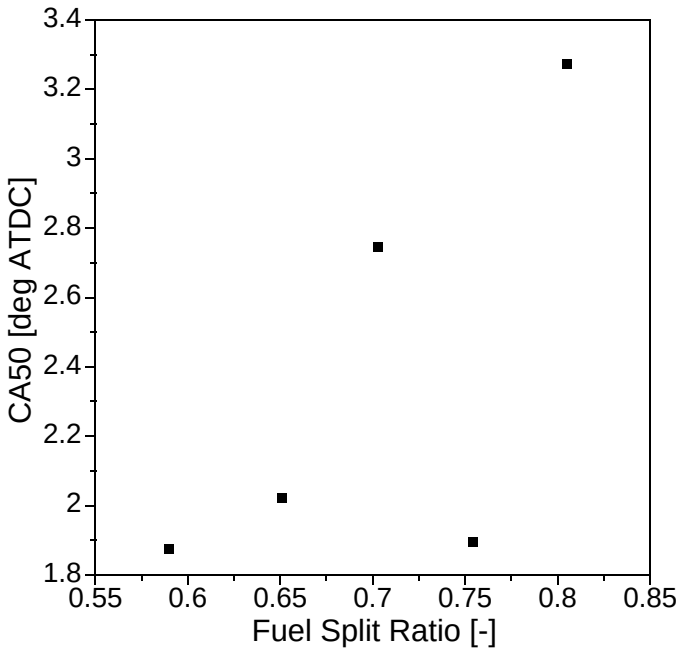

Figure 16: *CA50 during main combustion using EGR from NVOs with different fuel split ratios.*

NO_x removed from the EGR resulting in a CA50 1.9 deg ATDC.

These results can be used to explain why a decrease in fuel split ratio caused an advance in combustion phasing. At similar equivalence ratios and EVC temperatures the NVO heat release did not vary much when different mass of fuel was injected during NVO. This meant the heat released per mass of fuel was lower when more was added and the reactions did not proceed as far. The results suggest that for the same NVO heat release the fuel is more reactive if a larger percent of it undergoes a lower amount of reforming reactions. This agrees with the experimental and model results of cases 1-3. In cases 1, 4 and 5, more heat was released as the injection timing was advanced resulting in a less reactive charge. The increase in IVC temperature however had a stronger effect causing combustion phasing to advance. The fuel used in the experiments was 95 RON gasoline. This was simulated with a 60 RON PRF which may not capture the same properties however the simulated pressure profiles matched the trends seen in the experiment well.

4.3 NO Effect on Combustion Phasing

The effect of NO on combustion phasing was investigated using the SRM. The engine parameters and operating condition used are given in Table 5. The concentration of NO in the cylinder charge was varied between 0 and 503 ppm. A simulation was also run with 503 ppm NO_2 for comparison.

Table 5: *Engine specification and operating condition.*

Fuel	Iso-octane
Bore [mm]	102.0
Stroke [mm]	120.0
Con. rod length [mm]	192.0
CR	13.8
Disp. volume [cm3/cyl]	980.6
Lambda	2.7
Speed [RPM]	1200
Temp. at IVC [K]	430
Pres. at IVC [bar]	1.04
IVC [CAD BTDC]	155

The combustion phasing was advanced by the addition of NO to the charge, as can be seen from Figure 17. The effect is greatest at low levels of NO, which could be important for low NO_x HCCI combustion. The results are very similar to those that have been obtained experimentally, where a 250 ppm NO concentration advanced combustion phasing by roughly 6 CAD [14]. This was for an 84 RON PRF fuel in an HCCI engine operated at 900 RPM with a compression ratio of 13.6, air fuel equivalence ratio of 3.0 and inlet conditions of 1 bar and 100 °C.

4.4 NO_x in the NVO

The NO_x retained in the cylinder by early EVC is compressed with fresh fuel and the other exhaust gas components. The results from the calibrated engine simulation show NO_x present at EVC to disappear during NVO. A detailed flux analysis has shown the nitrogen in NO_x is mostly converted to HNCO and HCNO. Figure 18 shows the flux of nitrogen between species during NVO and the main reactions causing the flux. The arrow thickness corresponds qualitatively to the magnitude of the flux and the reactions in parentheses contribute to small amounts of the flux. The main reactions that occur are reactions (2), (3), (1) and (4).

$$\mathrm{HNO}\cdot + \mathrm{H}\cdot \rightleftharpoons \mathrm{NO} + \mathrm{H_2} \tag{2}$$

$$\mathrm{NO} + \mathrm{H}\cdot + \mathrm{M} \rightleftharpoons \mathrm{HNO}\cdot + \mathrm{M} \tag{3}$$

$$\mathrm{NO_2} + \mathrm{CH_3}\cdot \rightleftharpoons \mathrm{NO} + \mathrm{CH_3O}\cdot \tag{4}$$

The fluxes between NO and HNO were roughly twice those between NO and NO_2. The integrated flux of the reaction between NO and HCCO was roughly 20 times lower than those between NO and NO_2. The three reactions between NO_2 and HCCO all occurred at

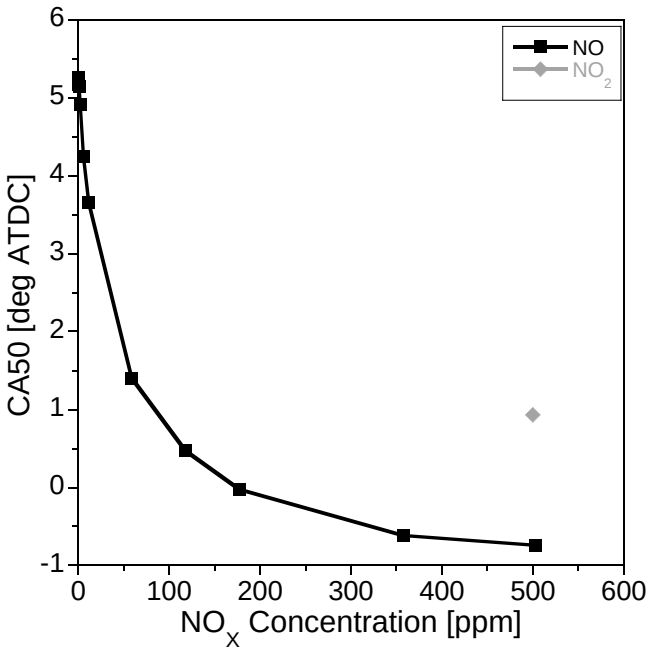

Figure 17: *CA50 plotted against the concentration of NO_x at IVC.*

about the same rate, which was around half that between NO and HCCO. The net fluxes are shown in Figure 19, where it can be seen the nitrogen from NO and NO_2 is mostly converted to HCNO and HNCO. The number of moles of NO, NO_2, HCNO and HNCO during NVO are shown in Figure 20.

The concentration of NO_x at EVC was varied to investigate the effect of NO_x on NVO heat release. The ratio of NO to NO_2 at EVC was left unchanged. The cumulative heat release during NVO is shown in Figure (21). It was found that an increase in EVC NO_x resulted in less NVO heat release, which is likely to cause a retarded combustion phasing. This is opposite to the effect when increased levels of NO_x are present at IVC. The rates of reactions 3 and 4 were extremely large in the NVO simulations. The overall effect of the two reactions is to combine the H radical to form molecular hydrogen. To asses their effect on NVO heat release simulations were done with them removed from the mechanism, referred to as mech2. Mech1 refers to the standard mechanism used. Figure 22 suggests these reactions were responsible for the decreased NVO heat release when EVC NO was increased. With the reactions removed an increase in NO caused an increase in NVO heat release compared to a decrease when the mechanism was not altered. This could have two important effects. Firstly the reduction in concentration of the H radical. Secondly, H_2 is known to reduce OH concentration by reaction (5) [29].

$$H_2 \quad + \quad OH\cdot \quad \rightleftharpoons \quad H_2O \quad + \quad H\cdot \tag{5}$$

The rate of this reaction was found to increase with a decrease in EVC NO_x, shown in Figure 23. Higher H_2 concentrations occur when less NO_x is present suggesting the hydrogen

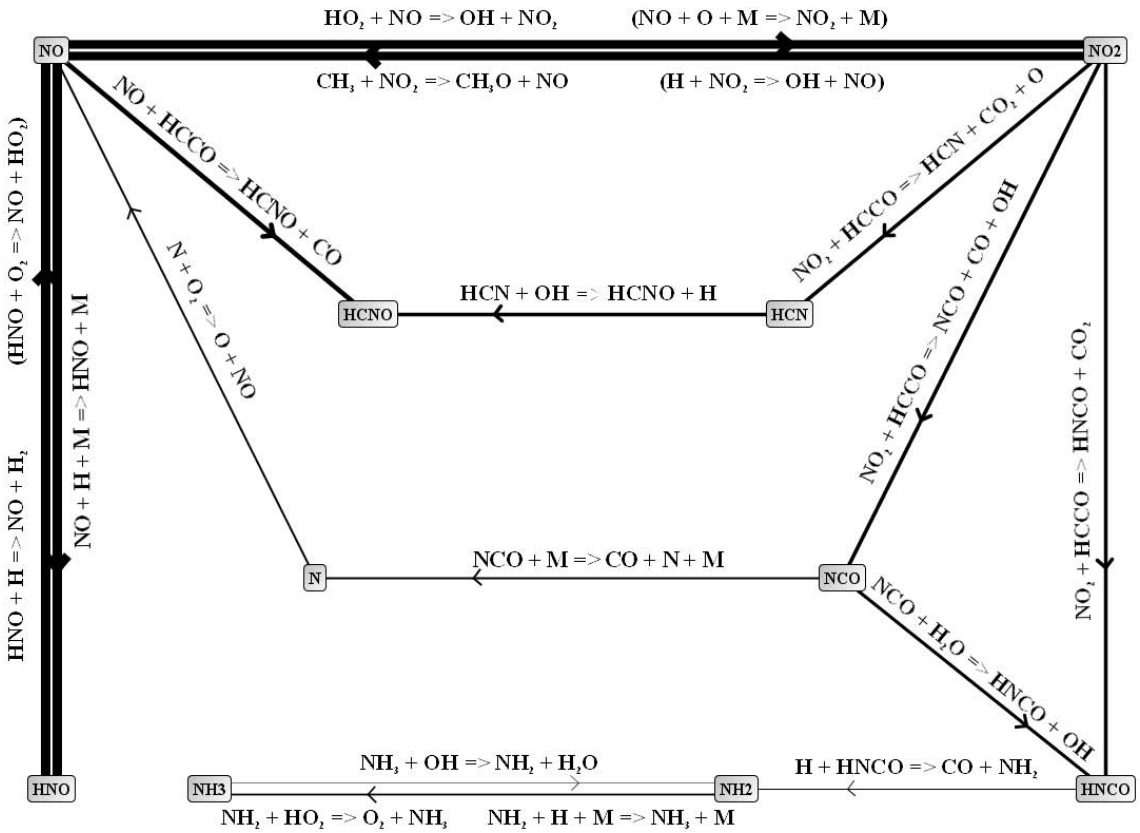

Figure 18: *Molar flux of nitrogen integrated over NVO and main reactions that contribute to each flux.*

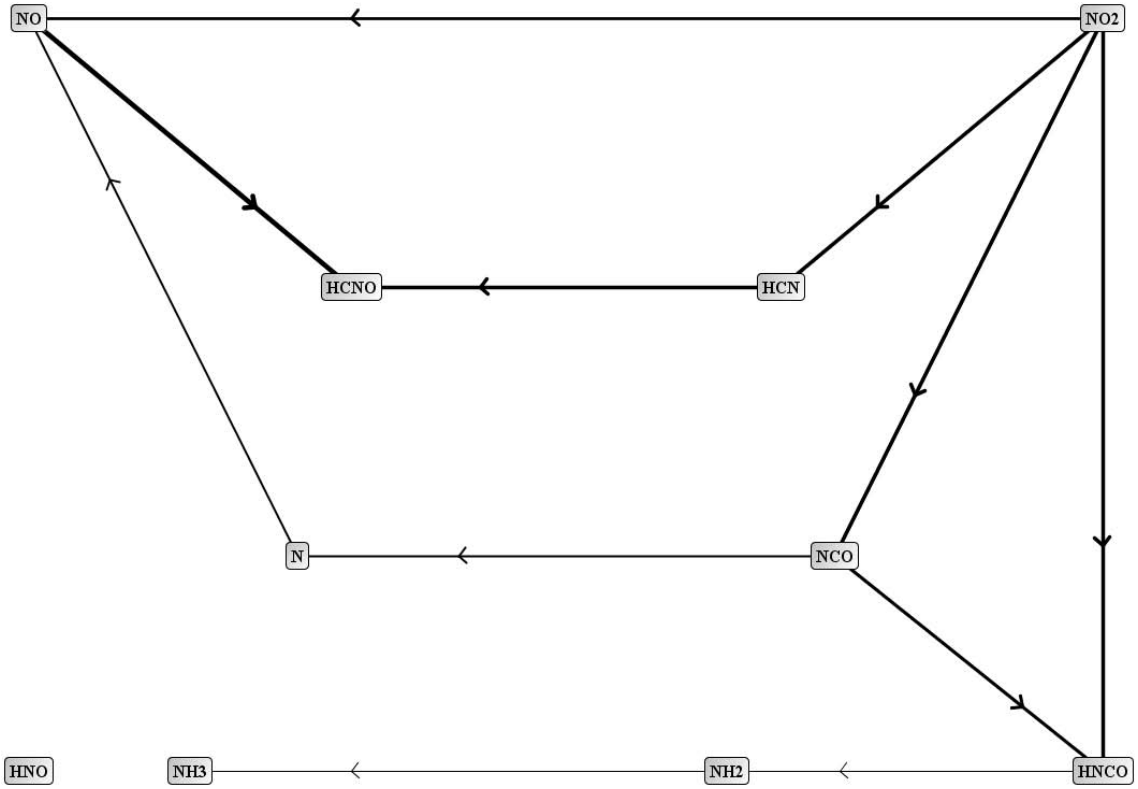

Figure 19: *Net molar flux of nitrogen integrated over NVO.*

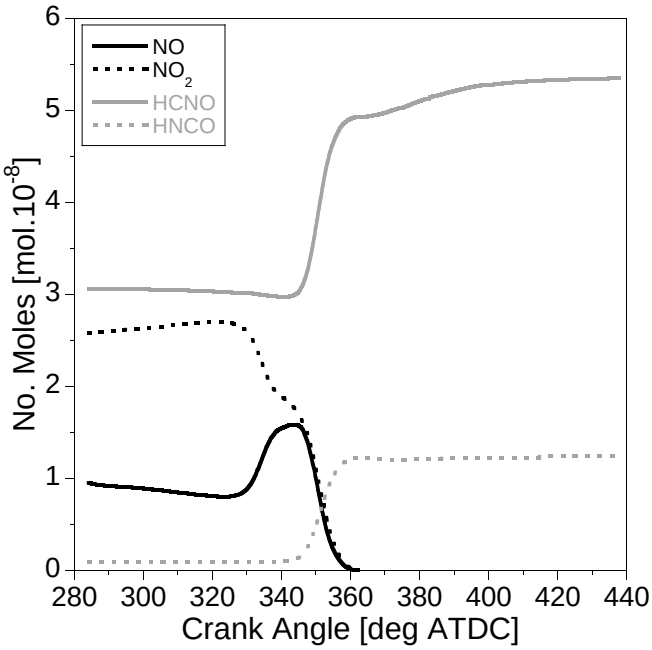

Figure 20: *Moles of NO, NO_2, HCNO and HNCO during NVO.*

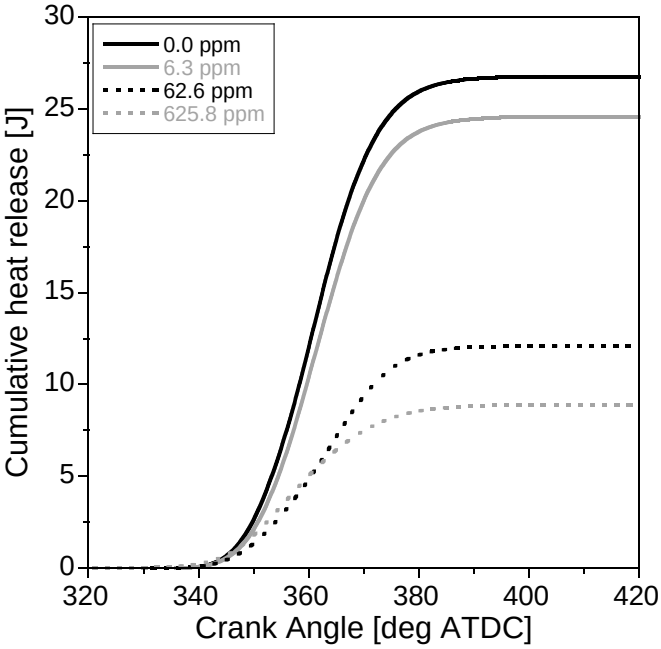

Figure 21: *Cumulative heat release during NVO with different initial NO_x concentrations.*

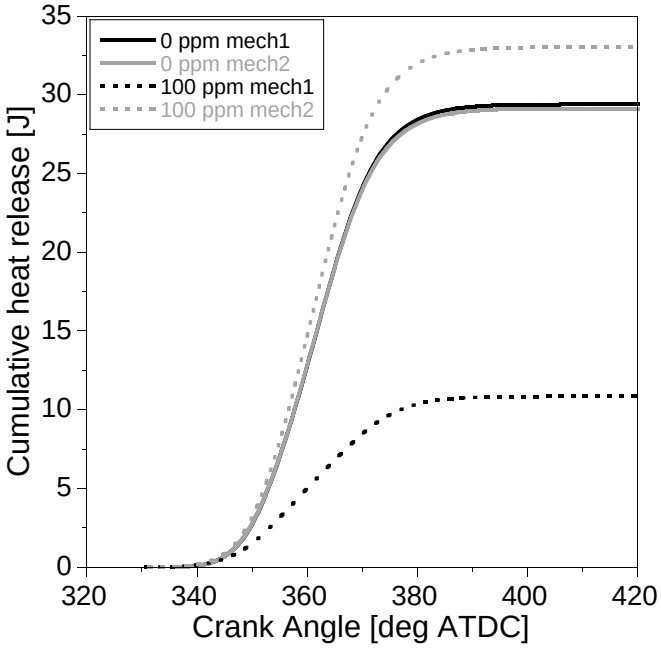

Figure 22: *Cumulative heat release during NVO with different initial NO concentrations and mechanisms.*

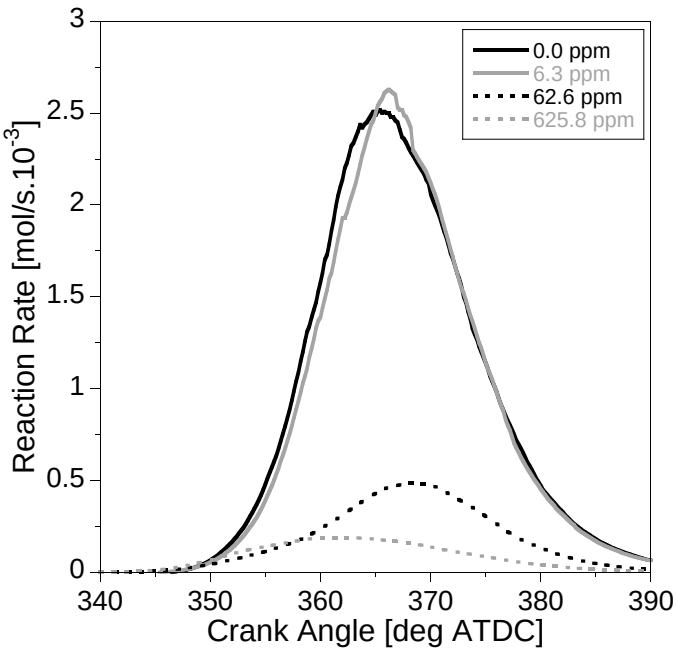

Figure 23: *Rate of reaction* (5) *during NVO with different initial NO_x concentrations.*

produced by reaction 2 is not the reason for a decrease in heat release. The reduction in the H radical concentration by reactions 2 and 3 is the likely cause. This effect may also contribute to CCV as advanced high temperature combustion produces more NO_x resulting in less heat release during NVO, a colder IVC temperature and a retarded combustion in the following cycle.

5 Conclusion

A stochastic reactor model (SRM) was calibrated to simulate an HCCI engine operated with NVO and a split fuel injection strategy. The model captures trends in combustion phasing and NO_x emissions at different pilot injection timings and fuel split ratios.

When 40 % of the fuel was injected during NVO, large peak pressure oscillations between consecutive cycles occurred in the simulation resulting in misfire in the 34th cycle. A high IVC temperature caused an advanced combustion phasing and a richer cylinder charge. The low O_2 concentration caused low NVO heat release. This in turn caused a retarded combustion phasing but a leaner mixture and high NVO heat release in the following cycle.

The chemical effect of fuel reforming on combustion phasing was investigated using 60 RON PRF and a detailed PRF mechanism. Increasing the O_2 concentration increased

NVO heat release at the conditions studied. The reformed fuel became less reactive the further reactions proceeded towards complete oxidation during NVO.

Advancing the pilot injection timing caused an increase in NVO heat release and advanced the main combustion phasing. The higher IVC temperature caused by increased NVO heat release had a greater effect on combustion phasing than the reactions during NVO that made the fuel less reactive.

Decreasing the fuel split ratio advanced combustion phasing. The percentage of reformed fuel increased but the reforming reactions did not proceed as far. The heat released during NVO and IVC temperature only showed a slight variation. The reduced progression of the oxidation reactions during NVO had a larger effect on the main combustion phasing than the increased mass of reformed fuel.

The effect of NO_x in the model was investigated. Increasing NO_x concentration at IVC advanced combustion phasing as has been reported in the literature. In the simulations the NO_x was consumed during NVO preventing its occurrence at IVC. Increased levels of NO_x were found to decrease NVO heat release due to reactions involving HNO consuming the reactive H radical.

List of Abbreviations and Symbols

Abbreviations

ABDC	After Bottom Dead Center
ATDC	After top dead centre
BBDC	Before Bottom Dead Center
BTDC	Before top dead centre
CAD	Crank angle degree
CA50	Crank Angle at 50 % heat release
CCV	Cycle to cycle variations
CFD	Computational fluid dynamics
CI	Compression Ignition
CIDI	Compression ignition direct injection
CPU	Central processing unit
CR	Compression ratio
DI	Direct Injection
EGR	Exhaust gas recycle
EMST	Euclidean minimum spanning tree
EVC	Exhaust valve close
EVO	Exhaust valve open
HCCI	Homogeneous charge compression ignition
ICE	Internal Combustion Engine
IVC	Inlet valve close
IVO	Inlet valve open
NVO	Negative valve overlap
OI	Octane Index
PDF	Probability density function
PRF	Primary reference fuel
RON	Research octane number
RPM	Revolutions Per Minute
SI	Spark ignition
SRM	Stochastic reactor model
TDC	Top dead centre
UHC	Unburned hydrocarbons

Symbols

ϕ	Fuel/air equivalence ratio [-]
λ	Air/fuel equivalence ratio [-]

References

[1] M. Kraft, P. Maigaard, F. Mauss, M. Christensen, and B. Johansson. Investigation of combustion emissions in a homogeneous charge compression injection engine: Measurements and a new computational model. *Proceedings of the Combustion Institute*, 28:1195–1201, 2000.

[2] P. Najt and D. Foster. Compression Ignited Homogeneous Charge Combustion. SAE Paper No. 830264, 1983.

[3] G. Shibata, K. Oyama, T. Urushihara, and T. Nakano. The Effect of Fuel Properties on Low and High Temperature Heat Release and Resulting Performance of an HCCI Engine. SAE Paper No. 2004-01-0553, 2004.

[4] J. Szybist and B. Bunting. The Use of Fuel Chemistry and Property Variations to Evaluate the Robustness of Variable Compression Ratio as a Control Method for Gasoline HCCI. SAE Paper No. 2007-01-0224, 2007.

[5] R. Stanglmaier, T. Ryan, and J. Souder. HCCI Operation of a Dual-Fuel Natural Gas Engine for Improved Fuel Efficiency and Ultra-Low NO_x Emissions at Low to Moderate Engine Loads. SAE Paper No. 2001-01-1897, 2001.

[6] R. Wagner, K. Edwards, C. Daw, J. Green Jr., and B. Bunting. On the Nature of Cyclic Dispersion in Spark Assisted HCCI Combustion. SAE Paper No. 2006-01-0418, 2006.

[7] C.S. Daw, R.M. Wagner, K.D. Edwards, and J.B. Green Jr. Understanding the transition between conventional spark-ignited combustion and HCCI in a gasoline engine. *Proceedings of the Combustion Institute*, 31:2887–2894, 2007.

[8] G. Tian, Z. Wang, Q. Ge, J. Wang, and S. Shuai. Mode Switch of SI-HCCI Combustion on a GDI Engine. SAE Paper No. 2007-01-0195, 2007.

[9] L. Koopmans and I. Denbratt. A Four Stroke Camless Engine, Operated in Homogeneous Charge Compression Ignition Mode with Commercial Gasoline. SAE Paper No. 2001-01-3610, 2001.

[10] L. Koopmans, O. Backlund, and I. Denbratt. Cycle to Cycle Variations: Their Influence on Cycle Resolved Gas Temperature and Unburned Hydrocarbons from a Camless Gasoline Compression Ignition Engine. SAE Paper No. 2002-01-0110, 2002.

[11] H. Persson, M. Agrell, J. Olsson, B. Johansson, and H. Ström. The Effect of Intake Temperature on HCCI Operation Using Negative Valve Overlap. SAE Paper No. 2004-01-0944, 2004.

[12] M. Sjöberg, J. Dec, and W. Hwang. Thermodynamic and Chemical Effects of EGR and its Constituents on HCCI Autoignition. SAE Paper No. 2007-01-0207, 2007.

[13] H. Zhao, Z. Peng, J. Williams, and N. Ladommatos. Understanding the Effects of Recycled Burnt Gases on the Controlled Autoignition (CAI) Combustion in Four-Stroke Gasoline Engines. SAE Paper No. 2001-01-3607, 2001.

[14] P. Risberg, D. Johansson, J. Andrae, G. Kalghatgi, P. Björnbom, and H. Ångström. The Influence of NO on the Combustion Phasing in an HCCI Engine. SAE Paper No. 2006-01-0416, 2006.

[15] O. Stenlåås, A. Gogan, R. Egnell, B. Sundén, and F. Mauss. The Influence of Nitric Oxide on the Occurrence of Autoignition in the End Gas of Spark Ignition Engines. SAE Paper No. 2002-01-2699, 2002.

[16] T. Urushihara, K. Hiraya, A. Kakuhao, and T. Itoh. Expansion of HCCI Operating Region by the Combination of Direct Fuel Injection, Negative Valve Overlap and Internal Fuel Reformation. SAE Paper No. 2003-01-0749, 2003.

[17] Y. Li, H. Zhao, N. Brouzos, T. Ma, and B. Leach. Effect of Injection Timing on Mixture and CAI Combustion in a GDI Engine with an Air-Assisted Injector. SAE Paper No. 2006-01-0206, 2006.

[18] R. Standing, N. Kalian, T. Ma, H. Zhao, M. Wirth, and A. Schamel. Effects of Injection Timing and Valve Timings on CAI Operation in a Multi-Cylinder DI Gasoline Engine. SAE Paper No. 2005-01-0132, 2005.

[19] B. Leach, H. Zhao, Y. Li, and T. Ma. Control of CAI Combustion Through Injection Timing in a GDI Engine With an Air-Assisted Injector. SAE Paper No. 2005-01-0134, 2005.

[20] T. Aroonsrisopon, D. Nitz, J. Waldman, D. Foster, and M. Iida. A Computational Analysis of Direct Injection During the Negative Valve Overlap Period in an Iso-Octane Fueled HCCI Engine. SAE Paper No. 2007-01-0227, 2007.

[21] J. Waldman, D. Nitz, T. Aroonsrisopon, D. Foster, and M. Iida. Experimental Investigation into the Effects of Direct Fuel Injection During the Negative Valve Overlap Period in a Gasoline Fueled HCCI Engine. SAE Paper No. 2007-01-0219, 2007.

[22] T. Guohong, W. Zhi, W. Jianxin, S. Shijin, and A. Xinliang. HCCI Combustion Control by Injection Strategy with Negative Valve Overlap in a GDI Engine. SAE Paper No. 2006-01-0415, 2006.

[23] H. Song and C. Edwards. Optimization of Recompression Reaction for Low-Load Operation of Residual-Effected HCCI. SAE Paper No. 2008-01-0016, 2008.

[24] G. Shaver, M. Roelle, P. Caton, N. Kaahaaina, N. Ravi, J. Hathout, J. Ahmed, A. Kojic, S. Park, C. Edwards, and J. Gerdes. A physics-based approach to the control of homogeneous charge compression ignition engines with variable valve actuation. *International Journal of Engine Research*, 6(4):361–375, 2005.

[25] S. Mosbach, A. Aldawood, and M. Kraft. Real-Time Evaluation of a Detailed Chemistry HCCI Engine Model Using a Tabulation Technique. *Combustion Science and Technology*, 180:1263–1277, 2008.

[26] S. Mosbach, H. Su, M. Kraft, A. Bhave, F. Mauss, Z. Wang, and J. Wang. Dual injection homogeneous charge compression ignition engine simulation using a stochastic reactor model. *International Journal of Engine Research*, 8(1):41–50, 2007.

[27] S. B. Pope. PDF methods for turbulent reactive flows. *Prog. Energy Combust. Sci.*, 11:119–192, 1985.

[28] S. Subramaniam and S. B. Pope. A Mixing Model for Turbulent Reactive Flows based on Euclidean Minimum Spanning Trees. *Combust. Flame*, 115:487–514, 1998.

[29] T. Shudo and H. Yamada. Hydrogen as an ignition-controlling agent for HCCI combustion engine by suppressing the low-temperature oxidation. Article in Press, 2007.